New Metal−Organic Frameworks for Chemical Fixation of CO2

Phuong T. K. Nguyen,[†,‡,#] Huong T. D. Nguyen,[†,‡,#] Hung N. Nguyen,[‡] Christopher A. Trickett,[§] Quang T. Ton,[‡] Enrique Gutiérrez-Puebla,[∥] M. Angeles Monge,[∥] Kyle E. Cordova,[§,⊥] and Felipe Gándara*,[∥]

[†]Center for Innovative Materials and Architectures (INOMAR), Vietnam National University—Ho Chi Minh City (VNU—HCM), Ho Chi Minh City 721337, Vietnam

[‡]Faculty of Chemistry, University of Science, Vietnam National University—Ho Chi Minh City, Ho Chi Minh City 721337, Vietnam

[§]Berkeley Global Science Institute, University of California—Berkeley, Berkeley, California 94720, United States

[∥]Departamento de Nuevas Arquitecturas en Química de Materiales, The Materials Science Factory, Instituto de Ciencia de Materiales de Madrid (ICMM-CSIC), Sor Juana Inés de la Cruz 3, Cantoblanco, 28049 Madrid, Spain

[⊥]Center for Research Excellence in Nanotechnology, King Fahd University of Petroleum and Minerals, Dhahran 31261, Saudi Arabia

S *Supporting Information*

ABSTRACT: A novel series of two zirconium- and one indium-based metal−organic frameworks (MOFs), namely, MOF-892, MOF-893, and MOF-894, constructed from the hexatopic linker, 1′,2′,3′,4′,5′,6′-hexakis(4-carboxyphenyl)benzene, were synthesized and fully characterized. MOF-892 and MOF-893 are two new exemplars of materials with topologies previously unseen in the important family of zirconium MOFs. MOF-892, MOF-893, and MOF-894 exhibit efficient heterogeneous catalytic activity for the cycloaddition of CO_2, resulting in a cyclic organic carbonate formation with high conversion, selectivity, and yield under mild conditions (1 atm CO_2, 80 °C, and solvent-free). Because of the structural features provided by their building units, MOF-892 and MOF-893 are replete with accessible Lewis and Brønsted acid sites located at the metal clusters and the non-coordinating carboxylic groups of the linkers, respectively, which is found to promote the catalytic CO_2 cycloaddition reaction. As a proof-of-concept, MOF-892 exhibits high catalytic activity in the one-pot synthesis of styrene carbonate from styrene and CO_2 without preliminary synthesis and isolation of styrene oxide.

KEYWORDS: *reticular chemistry, metal−organic frameworks, heterogeneous catalysis, carbon dioxide conversion, chemical fixation of CO₂*
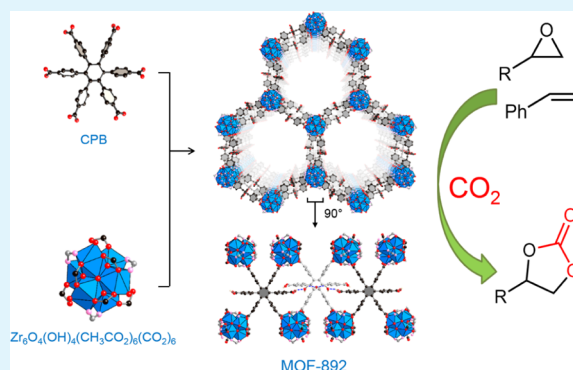
1. INTRODUCTION

Metal−organic frameworks (MOFs) are designable porous, crystalline materials that are constructed by combining inorganic metal clusters, denoted secondary building units (SBUs), and organic linkers via strong bonds.[1] The geometry and coordination number (points of extension) of the selected SBUs and organic linkers dictate the topological and structural features of the resulting frameworks, following the principles of reticular chemistry.[2] Using these principles, it is possible to prepare MOFs with the desired structural features for a given application. In the context of catalytic conversions, MOF materials can be constructed with large pore apertures and a high density of accessible metal sites,[3] by combining multiple active metal sites within a same framework[4] or by introducing active species in the MOF linkers[5] or inside their pores.[6]

Among the different metal cations that have been employed in the preparation of MOFs, zirconium has attracted much attention in recent years. This is in large part because many of the resulting MOFs have been proven to be stable in water and in low pH environments, making them suitable for applications in multiple fields.[7] Hence, following the report of UiO-66,[8] which has a 12-connected **fcu** topology, a number of new related materials have been published with increasing structural complexity, which arises from the use of different, multitopic organic linkers as well as from structural modifications in the inorganic SBUs.[9] These modifications may appear in the form of connectivity defects or as changes in the number or

Scheme 1. Hexatopic Linker, H$_6$CPB, Links Different Zirconium- and Indium-Based SBUs To Form MOF-892, MOF-893, and MOF-894, Which Adopt stp, hfp, and kgd Topologies, Respectively
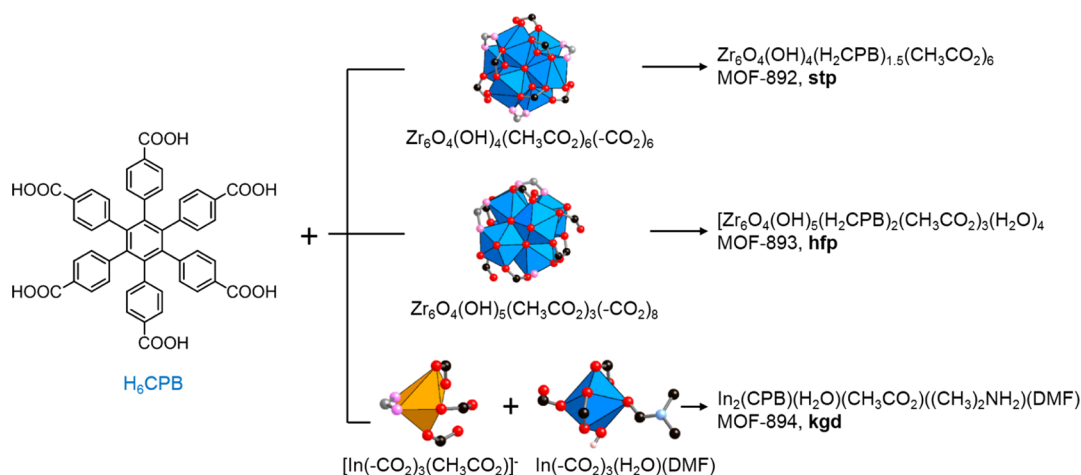
disposition of the SBU's points of extension.[10] Although most of the known zirconium MOFs are built from a related inorganic SBU consisting of six octahedrally arranged zirconium atoms joined by 8 μ^3 oxygen atoms (either O^{2-} or OH$^-$), the number of extension points for a given SBU can be modified to be 12, 10, 8, or 6.[11] Typically, this change is achieved by adjustments in the MOF synthetic conditions, for example, by the addition of modulating agents. These agents compete with the carboxylate groups of the organic linkers to occupy any of the 12 potential points of extension. Consequently, the structural variability of zirconium MOFs has significantly increased in recent years, and a large number of new materials formed by the combination of related Zr$_6$-based SBUs along with various multitopic organic linkers, producing networks with binodal topologies, including 12,4-connected (**ftw** and **ith**),[11,12] 8,4-c (**csq**, **flu**, and **sqc**),[11−13] 6,4-c (**she**),[14] or 6,3-c (**spn**),[15] among others have been reported.

On the other hand, the chemical exploitation of carbon dioxide, an abundant, available, and nontoxic source of carbon, has been widely employed as an alternative sustainable approach in the synthesis of fine chemicals.[16,17] Acid-catalyzed cycloaddition of CO$_2$ and epoxides is a highly atom-economical process to convert CO$_2$ into cyclic organic carbonates.[18] Numerous studies have been devoted to the development of efficient heterogeneous catalysts, including porous carbons,[19] zeolites,[20] ionic liquid-supported solids,[21] silica-supported solids,[22] polymers,[23] and MOFs.[24−35] However, there are some shortcomings when exploiting the chemical fixation of CO$_2$, such as the addition of organic solvent, the need for elevated pressure, harsh reaction conditions (high temperature and long reaction time), and/or low catalytic activity.[18,36] Thus, the development of new heterogeneous acidic catalysts to synthesize cyclic carbonates utilizing CO$_2$ as a building block is still of great interest. Moreover, developing a one-pot synthesis of cyclic carbonates from olefins and CO$_2$ is a highly desirable and economical approach because this reaction uses readily available olefins without the need for preliminary epoxide synthesis. However, typical oxidative carboxylation of olefins proceeds under high pressures of CO$_2$, resulting in low yields of carbonates due to the formation of a number of by-products.[37] Therefore, only a few studies of methodologies and catalysts conducting the

direct synthesis of cyclic carbonates from olefins have been reported thus far.[38,39]

Recently, we reported the use of 1′,2′,3′,4′,5′,6′-hexakis(4-carboxyphenyl)benzene (H$_6$CPB) as a linker in a series of MOFs with selective CO$_2$ sorption properties.[40] Herein, we report the synthesis and structural characterization of three new additional MOFs prepared with this H$_6$CPB linker, which acts as a tetratopic linker when combined with zirconium or as a hexatopic linker when combined with indium (Scheme 1). The new zirconium MOFs, denoted MOF-892 and MOF-893, are highly porous and exhibit network topologies that are unprecedented among the zirconium MOF family. Specifically, MOF-892 exhibits a 6,4-connected **stp** topology, based on the linking of trigonal prisms and rectangles, whereas MOF-893 exhibits a new topology, which we call **hfp**, based on 8- and 4-connected nodes. The indium-based MOF, denoted MOF-894, exhibits a structure based on the stacking of **kgd** layers.

Because of their suitable structural features, in particular the presence of accessible Lewis and Brønsted acid sites, the new MOFs have been evaluated as heterogeneous catalysts in CO$_2$ fixation of epoxides to form cyclic carbonates. All new MOFs show efficient catalytic performance under ambient pressure of CO$_2$, solvent-free, and mild conditions with an exceptional conversion of styrene oxide to styrene carbonate with high selectivity (86−99%) as well as yield (63−88%). MOF-892, with a mesoporous hexagonal channel of ca. 27 Å, permits the diffusion of large substrates and promotes effective activation through the synergistic effect of the Lewis and Brønsted acid sites in the CO$_2$ coupling reaction. Thus, we show that deactivation of the Brønsted acid sites by methylation of the free carboxylic groups results in a significant decrease of the MOF's catalytic performance. The activity of MOF-892 is wide in the scope of common epoxides and several cocatalysts, showing good to excellent activity. Also, MOF-892 outperforms other representative MOFs and homogeneous and heterogeneous catalysts. Furthermore, MOF-892 demonstrates remarkable catalytic activity for the one-pot synthesis of styrene carbonate formation from styrene without needing to isolate styrene oxide. Accordingly, MOF-892 is highlighted as a robust MOF that can effectively promote the oxidative carboxylation of styrene and CO$_2$ under mild conditions and short reaction time, compared to other reported MOF catalysts.[41,42]

2. EXPERIMENTAL SECTION

2.1. Materials and General Procedures. The synthesis of H_6CPB linker was carried out according to a previously reported procedure.[40] All chemicals for MOF synthesis and catalytic reactions were purchased and used without further purification. For comparison studies, commercially available porous heterogeneous catalysts [silica–alumina, Y-zeolite, HKUST-1 (Basolite C300), MOF-177 (Basolite Z377), ZIF-8 (Basolite Z1200), and Al-MIL-53 (Basolite A100)] were purchased and reactivated to obtain guest-free materials prior to use. MOF-890, UiO-67-bpydc, and Mg-MOF-74 were prepared according to reported procedures (Supporting Information, section S1).

Elemental microanalyses (EAs) were performed in the Instituto de Ciencia de Materiales de Madrid (ICMM-CSIC), using a LECO CHNS-932 analyzer. Fourier transform infrared (FT-IR) spectra were obtained using KBr pellets on a Bruker VERTEX 70 system, and the output signals were described as follows: vs, very strong; s, strong; m, medium; sh, shoulder; w, weak; vw, very weak; and br, broad. Thermal gravimetric analyses (TGAs) were performed on a TA Q500 thermal analysis system with the samples held in a platinum pan with continuous airflow. Low-pressure N_2 and CO_2 adsorption isotherms were recorded on a Micromeritics 3Flex instrument. A liquid N_2 bath was used for measurements at 77 K, and a water circulator was used for measurements at 273, 283, and 298 K. For all sorption measurements, He was used to estimate the dead space. ^1H and ^{13}C nuclear magnetic resonance (NMR) spectra were recorded on a Bruker ADVANCE II 500 MHz spectrometer. An Agilent gas chromatography (GC) System 19091s-433 equipped with a mass selective detector Agilent 5973N instrument [GC–mass spectrometry (GC–MS)] was used to confirm the products using a capillary HP-5MS 5% phenyl methyl silox column (30 m × 250 μm × 0.25 μm). The conversion, selectivity, and yield of catalytic reactions were determined by the Agilent GC system 123-0132 equipped with a flame ionization detector (FID) and a capillary DB-1ms column (30 m × 320 μm × 0.25 μm). Biphenyl was used as an internal standard for these measurements.

2.2. X-ray Diffraction Analysis. Single-crystal X-ray diffraction (SXRD) data for MOF-892 and MOF-893 were collected at beamline 11.3.1 of the Advanced Light Source at Lawrence Berkeley National Laboratory, equipped with a Bruker PHOTON 100 CMOS area detector using synchrotron radiation (10−17 keV), at 0.7749(1) Å. X-ray diffraction data for MOF-894 were obtained with a Bruker four circle kappa-diffractometer equipped with a Cu INCOATED microsource, operated at 30 W power (45 kV, 0.60 mA) to generate Cu Kα radiation (λ = 1.54178 Å), and a Bruker VÅNTEC 500 area detector (MICROGAP Technology). The raw data were processed with the Bruker APEX3 software package[43] and then integrated with the Bruker SAINT package[44] using a narrow-frame algorithm— corrected for absorption using the SADABS procedure.[45] The structures were solved by intrinsic phasing methods. The refinement was performed by full-matrix least-squares on F^2 (SHELXL-2014)[46] using the Olex^2 software package.[47] To improve the refinement, highly disordered guest molecules occupying the cavities of the structure, which could not be modeled, were accounted for using solvent masking. Powder X-ray diffraction (PXRD) data were collected using a Bruker D8 ADVANCE employing Ni-filtered Cu Kα (λ = 1.54178 Å). The system was also outfitted with an antiscattering shield that prevents incident diffuse radiation from hitting the detector. The 2θ range was 3°−50° with a step size of 0.02° and a fixed counting time of 1 s per step.

2.3. Synthesis of MOF-892. A 0.05 M stock solution of zirconium(IV) oxychloride octahydrate in N,N'-dimethylformamide (1.6 mL; DMF) was added to a 10 mL Pyrex tube (o.d. × i.d. = 1.2 cm × 1.0 cm), which was preloaded with H_6CPB (16 mg, 0.020 mmol). This was followed by the addition of 1.50 mL of a 0.30 M stock solution of 4-nitrobenzoic acid in DMF as well as 2.5 mL of glacial acetic acid. The tube was sonicated for 30 min and then flash frozen and sealed. Subsequently, the reaction mixture was heated at 120 °C for 4 d to produce colorless hexagonal bipyramid-shaped

crystals. The crystals were then thoroughly washed with anhydrous DMF (4 × 5 mL per day for a total of 3 d). The DMF-washed sample of MOF-892 was then immersed in anhydrous methanol (4 × 5 mL per day over a period of 3 d). The MeOH-exchanged sample was activated by the supercritical CO_2 method and then heated at 50 °C under vacuum for 24 h. Calcd for $Zr_6C_{84.6}H_{82.4}N_{0.2}O_{48.2}$ = $[Zr_6O_4(OH)_4(H_2CPB)_{1.5}(CH_3CO_2)_6]\cdot10H_2O\cdot0.2DMF$: C, 41.98; H, 3.43; N, 0.12%. Found: C, 41.43; H, 3.17; N, 0.40%. FT-IR (KBr, 4000−400 cm^{-1}): 3685 (br), 1704 (m), 1525 (s), 1385 (br), 1275 (w), 1181 (w), 1149 (vw), 1103 (vw), 1018 (s), 862 (s), 740 (s), 650 (w).

2.4. Synthesis of MOF-893. A 0.05 M stock solution of zirconium(IV) oxychloride octahydrate in DMF (0.60 mL) was added to a 10 mL Pyrex tube (o.d. × i.d. = 1.2 cm × 1.0 cm), which was preloaded with H_6CPB (17 mg, 0.021 mmol). This was followed by the addition of 0.59 mL of a 0.45 M stock solution of benzoic acid in DMF, 1.8 mL of anhydrous DMF, and last 1.9 mL of glacial acetic acid. The tube was sonicated for 30 min and then flash frozen and sealed. Subsequently, the reaction mixture was heated at 120 °C for 5 d to produce colorless rectangular-shaped crystals. The crystals were then thoroughly washed with DMF (4 × 5 mL per day for a total of 3 d). To yield guest-free material, DMF-washed MOF-893 was subsequently immersed in anhydrous methanol (4 × 5 mL per day over a period of 3 d). The solvent-exchanged sample was activated under vacuum at ambient temperature for 12 h, followed by heating at 100 °C under vacuum for an additional 24 h. Calcd for $Zr_6C_{102.6}H_{107.4}N_{0.2}O_{59.2}$ = $[Zr_6O_4(OH)_4(H_2CPB)_2(CH_3CO_2)_3(OH)-(H_2O)_4]\cdot16H_2O\cdot0.2DMF$: C, 43.42; H, 3.81; N, 0.10%. Found: C, 42.89; H, 3.35; N, 0.48%. FT-IR (KBr, 4000−400 cm^{-1}): 3431 (br), 1694 (w), 1606 (s), 1534 (m), 1405 (br), 1273 (vw), 1178 (m), 1148 (vw), 1102 (w), 1018 (m), 862 (m), 790 (vw), 744 (s), 648 (w), 477 (w).

2.5. Synthesis of MOF-894. Indium(III) nitrate hydrate (12 mg, 0.040 mmol) and H_6CPB (16 mg, 0.020 mmol) in 0.5 mL of DMF were added to a 4 mL vial. This was followed by the addition of 0.5 mL of H_2O, 0.5 mL of acetonitrile, and last 0.5 mL of glacial acetic acid. The mixture was then sonicated for 15 min and heated at 90 °C for 2 d to produce colorless block-shaped crystals. The crystals were then thoroughly washed with DMF for 3 d and immersed in anhydrous ethanol for 3 d. The solvent-exchanged sample was activated under vacuum at ambient temperature for 12 h, followed by heating at 150 °C under vacuum for an additional 24 h. Calcd for $C_{58}H_{51}In_2N_3O_{17}$ = $[In_2(C_{48}H_{24}O_{12})(H_2O)(CH_3CO_2)((CH_3)_2NH_2)-(DMF)]\cdot DMF$: C, 53.93; H, 3.98; N, 3.25%. Found: C, 54.02; H, 3.99; N, 3.17%. FT-IR (KBr, 4000−400 cm^{-1}): 3454 (br), 1656 (w), 1609 (s), 1541 (br), 1404 (w), 1384 (w), 1278 (vw), 1180 (m), 1150 (vw), 1101 (w), 1018 (s), 880 (br), 866 (br), 757 (s), 611 (w), 488 (w).

2.6. Catalytic Cycloaddition of CO_2 to Epoxides. All of the catalytic reactions were carried out with a balloon pressure of CO_2 (1 atm) in a 25 mL Schlenk tube. Prior to carrying out the catalytic reactions, the catalysts were activated to remove the guest molecules. In a typical experiment, the appropriate epoxide (6.87 mmol), activated MOF catalyst (0.32 mol % ratio, based on the molecular weight from $[Zr_6O_4(OH)_4(H_2CPB)_{1.5}(CH_3CO_2)_6]\cdot10H_2O\cdot0.2DMF$, $[Zr_6O_4(OH)_4(H_2CPB)_2(CH_3CO_2)_3(OH)(H_2O)_4]\cdot16H_2O\cdot0.2DMF$, or $[In_2(C_{48}H_{24}O_{12})(H_2O)(CH_3CO_2)((CH_3)_2NH_2)(DMF)]\cdot DMF$ for MOF-892, MOF-893, or MOF-894, respectively), and tetrabutylammonium bromide (nBu_4NBr, 0.068 mmol, 1 mol %) were added to the Schlenk tube. The mixture was then evacuated and purged with CO_2 three times prior to maintaining a constant pressure (1 atm) via a balloon filled with CO_2. At this point, the reaction mixture, under an atmosphere of CO_2, was stirred at 80 °C and monitored by GC−MS with aliquots taken at regular time intervals. After a certain time had elapsed, the mixtures were cooled to room temperature and the unreacted CO_2 was vented. The catalyst was then separated by centrifugation, and an aliquot of the supernatant was analyzed by GC−FID using biphenyl as the internal standard to determine the catalytic conversion, selectivity, and yield of reaction. The crude products were extracted and purified by silica gel column
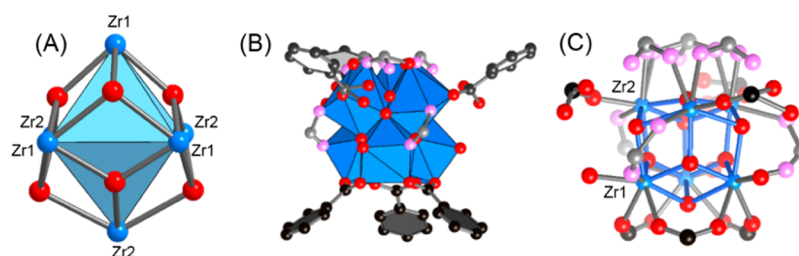
Figure 1. (A) Overall geometry of the $Zr_6(\mu_3\text{-}O)_4(\mu_3\text{-}OH)_4$ SBU observed in MOF-892. (B) There are three bridging bidentate (represented by black-filled benzyl rings) and three monodentate carboxylates (represented by white-filled benzyl rings) in each SBU. (C) $Zr_6O_4(OH)_4(CH_3CO_2)_6(CO_2)_6$ SBU represented in a ball-and-stick format. Atom colors: Zr, blue polyhedra or spheres; C and O atoms, black and red spheres, respectively; and acetate C and O atoms, gray and pink spheres, respectively; all H atoms are omitted for clarity.

chromatography to afford the pure products as confirmed by FT-IR, ^{1}H NMR, ^{13}C NMR, and GC−MS. The recovered catalyst was reactivated by washing with DMF (3 × 5 mL) and MeOH (4 × 5 mL), followed by heating under dynamic vacuum (same conditions used for the parent catalyst) prior to reuse in successive cycles.

2.7. Methyl Esterification of MOF-892. Activated MOF-892 (100 mg) was dispersed in 12 mL of a toluene/methanol (2:1 v/v) solution in a 20 mL scintillation vial. A 40 μL aliquot of 2.0 M trimethylsilyldiazomethane (TMS-CHN$_2$) solution in diethyl ether was added to the solution, and the samples were maintained at 0 °C by a water circulator. After 24 h, the reaction solution was decanted and the sample was soaked in anhydrous MeOH (3 × 5 mL) to remove any trace reactants. To yield solvent-free methyl ester materials, the MeOH-washed MOF-892 was activated using super-critical CO$_2$ drying, followed by heating at 50 °C under vacuum for 24 h.

2.8. Catalytic Cycloaddition of CO$_2$ to Styrene. The catalytic cycloaddition of CO$_2$ to styrene reactions was carried out using a balloon pressure of CO$_2$ (1 atm) in a 25 mL Schlenk tube. Prior to carrying out the catalytic reactions, the catalysts were activated to remove the guests. In a model experiment, the reactions were conducted using styrene (1.30 mmol), MOF-892 (6 mol % ratio, based on the molecular weight of $[Zr_6O_4(OH)_4(H_2CPB)_{1.5}(CH_3CO_2)_6]\cdot10H_2O\cdot0.2DMF)$, *tert*-butyl hydroperoxide solution in decane (TBHP, 3.92 mmol), and nBu$_4$NBr (0.104 mmol, 8 mol %). The mixture was then evacuated and purged with CO$_2$ three times prior to maintaining a constant pressure (1 atm) via a balloon filled with CO$_2$. At this point, the reaction mixture, under an atmosphere of CO$_2$, was stirred at 80 °C and monitored by GC−MS with aliquots taken at regular time intervals. After a certain time had elapsed, the mixtures were cooled to room temperature and the unreacted CO$_2$ was vented. The catalyst was then separated by centrifugation, and an aliquot of the supernatant was analyzed by GC−FID using biphenyl as the internal standard to determine the catalytic conversion, selectivity, and yield of reaction.

3. RESULTS AND DISCUSSION

3.1. Crystal Structures of MOF-892 to MOF-894. The topologies of MOF-891, MOF-892, and MOF-893 were evaluated using the TopsoPro (v.5.0) software program.[48] The simplification method, "cluster", was used for the abstraction of linkers and metal clusters.

3.1.1. MOF-892. Prior to performing SXRD analysis, single crystals of MOF-892 were washed and immersed in N,N'-dimethylacetamide (DMA) to remove any remaining un-reacted H$_6$CPB. MOF-892 crystallizes in the hexagonal system, $P6_3/m$ space group (no. 176), with lattice parameters $a = b = 32.2282(14)$ Å and $c = 26.5476(12)$ Å (Supporting Information, section S2). Structural analysis of MOF-892 revealed that each octahedron of zirconium atoms is capped by 4 μ_3 oxo and 4 μ_3 hydroxy groups with different bond lengths and angles (Figure 1A). There are two crystallographically

independent zirconium atoms in the SBU. Specifically, the first, Zr$_1$, is bound to three bridging carboxylate groups. The second, Zr$_2$, is connected to three monodentate carboxylates whose free oxygen atoms are found to be disordered over two positions with an occupancy of 50% in each position (Figure 1B). Additionally, the SBU of MOF-892 contains three acetate anions that bridge Zr$_1$ and Zr$_2$ atoms as well as three acetate anions bound to Zr$_2$, which are also found to be disordered over two positions. It is noted that positional disorder of several oxygen atoms found in the SBU were observed during crystal structure refinement. The remaining sites of the coordination sphere were completed by three DMA molecules (Figure 1C).

When taken together, the spatial arrangement of the linker's six carboxyl groups results in a simplified SBU adopting a distorted trigonal prismatic geometry. It is noted that this spatial arrangement is unprecedented for zirconium-based MOFs, as previous examples of 6-connected SBUs have all adopted hexagonal planar[14,49−51] or trigonal antiprismatic[52] geometries. With respect to the geometry and connectivity of the organic linker, because two out of the six carboxylic acid groups remains uncoordinated, the linker can be simplified to a 4-c rectangular geometry (Figure 2A). Therefore, the resulting structure can be described as exhibiting a **stp** topology, which is an edge-transitive 6,4-connected network as described in the Reticular Chemistry Structure Resource database.[53] The overall structure of MOF-892 contains large hexagonal one-dimensional (1D) channels with a void space of 72.8%, in its fully desolvated form, as determined by PLATON.[54] The metrics of the pore aperture calculated from the crystal structure are 24 × 27 Å^2 along the c-axis (Figure 2B,C and Supporting Information, section S2).

3.1.2. MOF-893. SXRD analysis reveals that MOF-893 crystallizes in the monoclinic system, space group $C2/c$ (no. 15) with lattice constants $a = 24.6147(9)$, $b = 69.169(2)$, $c = 19.5485(7)$ Å, and $\beta = 92.081(2)°$ (Supporting Information, section S2). To form the Zr$_6$O$_8$ cluster core observed in the structure of MOF-893, there exists six crystallographically unique zirconium atoms, which are connected to 8 μ^3 O atoms. Differences in the bond distances and angles between the Zr and the μ^3 O atoms reveal the presence of four O^{2-} and four OH$^-$ moieties (Figure 3A). Furthermore, eight carboxylate groups from the organic linkers coordinate to the inorganic SBUs, with five of these coordinating in a bridging fashion and three coordinating in a monodentate manner (Figure 3B). Finally, three additional acetic acid molecules and one OH$^-$ group are present in the SBU, thus preserving the charge balance. The coordination environment is completed by four additional water ligands (Figure 3C). Similar to the structure
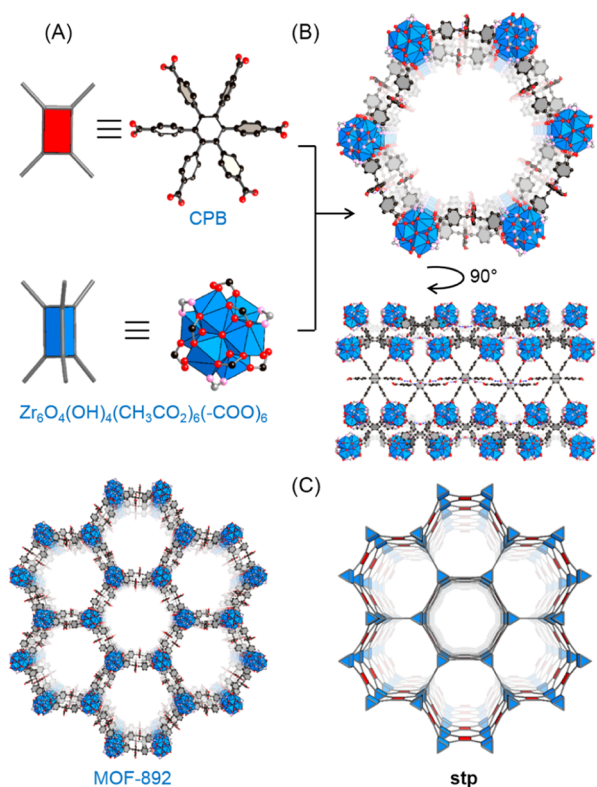
Figure 2. Crystal structure of MOF-892. (A) Linking of rectangular H_2CPB^{4-} and trigonal prismatic $Zr_6O_4(OH)_4(CH_3CO_2)_6(CO_2)_6$ SBUs results in (B) MOF-892. (C) Structure of MOF-892 adopts the **stp** topology. Atom colors: Zr, blue polyhedral; C and O atoms, black and red spheres, respectively; and acetate C and O atoms, gray and pink spheres, respectively; all H atoms are omitted for clarity.

Figure 4. Crystal structure of MOF-893. (A) Linking of rectangular H_2CPB^{4-} and distorted cube-shaped $Zr_6O_4(OH)_5(CH_3CO_2)_3(CO_2)_8$ SBUs results in (B) MOF-893. (C) Structure of MOF-893 adopts the new **hfp** topology. Atom colors: Zr, blue polyhedra; C and O atoms, black and red spheres, respectively; and acetate C and O atoms, gray and pink spheres, respectively; all H atoms are omitted for clarity.

of MOF-892, the organic linkers are 4-c, with two remaining carboxylic groups being uncoordinated. Topological analysis reveals that the three-dimensional framework of MOF-893 adopts a new topology, termed **hfp**, with a point symbol of $(4^{14}6^{12}8^2)(4^26^4)(4^46^2)$ due to the linkage of 8-c SBUs and three distinct types of 4-c linkers (Figure 4A,C and Supporting Information, Figure S5). Systre[55] analysis of this new topological type performed indicated that the maximum symmetry embedding of this network is in the orthorhombic *Cmcm* space group (no. 63), where the 4-c nodes adopt a rectangular shape and the 8-c node exhibiting an irregular, distorted cube shape.

Along the *a*-axis, MOF-893 displays triangular 1D channels, which have a maximum pore aperture diameter of 8.6 × 9.9 Å^2.

Half of the channels are replete with uncoordinated benzoic carboxyl groups from the H_2CPB^{4-} linker, resulting in narrower pore aperture diameters. It is noted that all channels and pores are blocked along the *b*-axis. With respect to the *c*-axis, there are four different types of channels: (i) the largest channel aperture adopts a hexagonal shape, but it is partly hindered by two benzoic carboxyl groups from two H_6CPB molecules, thus resulting in an aperture diameter of 6.3 × 15.1 Å^2; (ii) two smaller channels with rhomboidal and triangular shapes have diameters of 5.6 × 7.3 and 3.0 × 3.1 Å^2, respectively; and (iii) the smallest channel along the *c*-axis is rhomboidal but is obstructed by benzoic acid moieties from neighboring linkers (Figure 4B). The void space of MOF-893, in fully desolvated form, is ∼51.3% per PLATON calculations.[54]

3.1.3. MOF-894. SXRD analysis reveals that MOF-894 crystallizes in the monoclinic space group $P2_1/c$ (no. 14) with
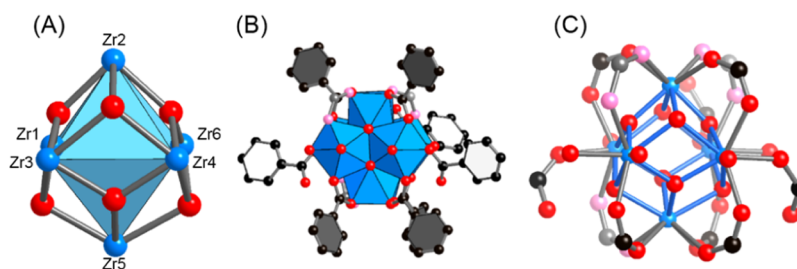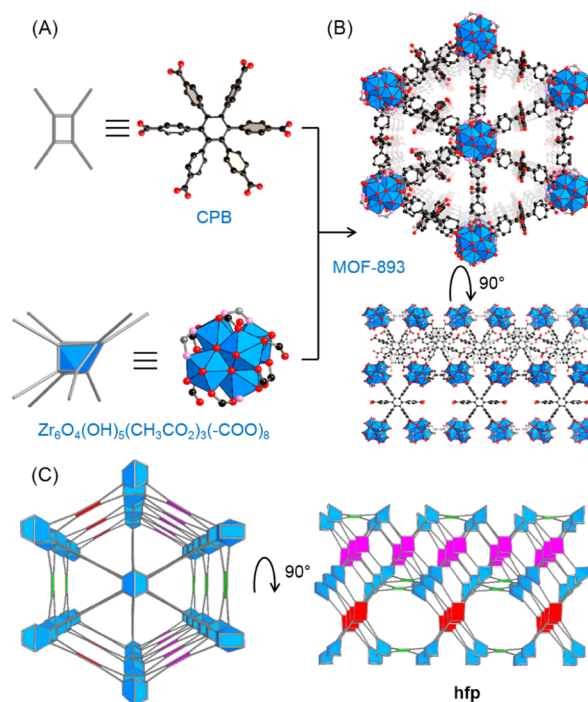

Figure 3. (A) $Zr_6(\mu_3\text{-}O)_4(\mu_3\text{-}OH)_4$ cluster core in MOF-893. (B) Five bridging dimonodentate (represented in black benzyl ring) and three monodentate carboxylates (represented in white benzyl ring) connections. (C) Three additional acetic acid molecules and one OH$^-$ group bridge Zr atoms in each SBU. Atom colors: Zr, blue polyhedra or spheres; C and O atoms, black and red spheres, respectively; and acetate C and O atoms, gray and pink spheres, respectively; all H atoms are omitted for clarity.

unit cell parameters $a = 12.666(3)$, $b = 29.888(6)$, $c = 15.424(3)$ Å, and $\beta = 112.43(3)°$ (Supporting Information, section S2). It is well-known that indium-based MOFs exhibit a larger variability of SBUs than zirconium MOFs. As such, the monoatomic indium SBU is among the most commonly found.[56] In MOF-894, there are two crystallographically distinct inorganic SBUs (Figure 5A). In one of these,
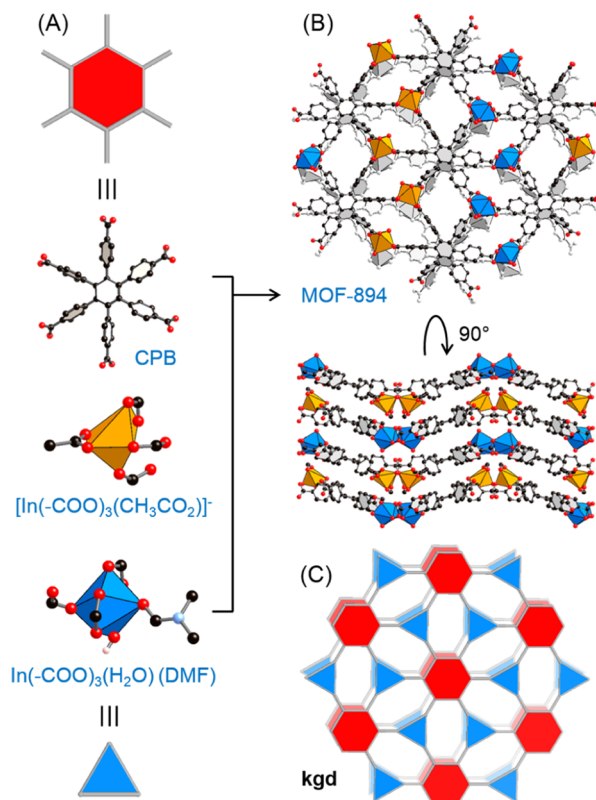

Figure 5. Crystal structure of MOF-894. (A) Linking of hexagonal CPB^{6-} linkers and triangular $[In(-CO_2)_3(CH_3CO_2)]^-$ and In-$(-CO_2)_3(H_2O)(DMF)$ SBUs results in (B) MOF-894. (C) Structure of MOF-894 adopts the **kgd** topology. Atom colors: In, blue and orange polyhedra; C, black; and O, red; all H atoms are omitted for clarity.

$In(-CO_2)_3(H_2O)(DMF)$, a In^{3+} cation is seen with a coordination number of seven. The coordination sphere is composed of three carboxyl groups from the linker in addition to two solvent ligands: one water and one DMF. In the second SBU, $[In(-CO_2)_3(CH_3CO_2)]^-$, a In^{3+} cation is coordinated by three carboxylate groups from the linker with an additional acetate anion present to produce an overall anionic framework. Dimethylammonium cations are located within the pores, which serve as counterions. The linkers are fully deprotonated CPB^{6-}. The resulting structure consists of two-dimensional layers parallel to the *ab* plane, with the topology identified as **kgd**. For this topological determination, the CPB^{6-} linkers serve as 6-c nodes and the indium SBUs are 3-c (Figure 5B,C). The layers stack along the crystallographic *c*-axis, with the inorganic SBUs disposed in an alternating ABAB sequence.

3.2. Other Structural Characterization, Porosity, and CO_2 Adsorption Properties.
As a result of the structure's large pore characteristic, the activation of MOF-892 was achieved by a supercritical CO_2 drying procedure, after carrying out a solvent-exchange process with anhydrous

methanol. MOF-893 and MOF-894 were activated after solvent exchanging with anhydrous methanol for 3 d, followed by conventional evacuation at room temperature, and later heating to afford guest-free compounds for evaluation of their permanent porosity. The crystallinity of the activated materials was proved by the powder X-ray diffraction (PXRD) analysis. The obtained powder diffraction patterns were in good agreement with those simulated from the single-crystal structures, thus confirming the maintenance of their structural integrity upon activation (Supporting Information, section S3, Figures S8−S10). It is noted that structural maintenance was also retained after immersing MOF-892, MOF-893, and MOF-894 in water at room temperature for 1 month as demonstrated by the PXRD analysis (Supporting Information, Figures S11−S13).

The thermal robustness of MOF-892 to MOF-894 was demonstrated by performing TGA under airflow (Supporting Information, section S3). For each MOF, the TGA curve exhibited only minor weight losses up to the 350−400 °C range, thus highlighting the high thermal stability of these materials. The major weight loss observed at ∼350 °C in each TGA is attributed to the framework destruction (Supporting Information, Figures S14−S16). Analysis of the residual metal oxide for MOF-892 (34.4%), MOF-893 (32.9%), and MOF-894 (22.5%) was confirmed as consistent with the calculated value derived from the EA (33.2, 30.0, and 21.5%, respectively). FT-IR measurements were performed on activated samples of MOF-892 and MOF-893 to assess the presence of coordinated carboxylate and free carboxylic acid moieties. Accordingly, the carboxyl OH stretching frequency of H_6CPB (3439 cm^{-1}) shifted to lower wavenumbers (3410 and 3402 cm^{-1} for MOF-892 and MOF-893, respectively) owing to extensive hydrogen bonding in these MOFs. The C=O stretching and C−OH bending vibrations, characteristic of carboxylic acids, appear at 1700 and 1270 cm^{-1}, respectively. These characteristic absorption bands appeared with weak intensities and were slightly shifted for MOF-892 and MOF-893, thus, indicating the existence of free carboxylic acid groups in these frameworks (Supporting Information, Figure S17).

The permanent porosity of MOF-892 to MOF-894 was proven by N_2 adsorption isotherms at 77 K (Supporting Information, section S4). As such, the isotherm of MOF-892 revealed a steep increase at $P/P_0 = 0.15$ with the resulting profile being characterized as type-IV (mesoporous). On the other hand, MOF-893 exhibited a fully reversible type-I isotherm, with steep N_2 uptake in the low-pressure region ($P/P_0 < 0.06$) (Supporting Information, Figure S18), indicative of microporosity. The Brunauer−Emmett−Teller (BET) (Langmuir) and surface areas of MOF-892 and MOF-893 were calculated as 1904 (2165) and 760 (850) m^2 g^{-1}, respectively. Finally, MOF-894 exhibited only a small N_2 uptake in the low-pressure region with a corresponding surface area of 5 m^2 g^{-1}. The small amount of adsorbed N_2 by MOF-894 is largely attributed to the presence of counterions filling the small pores. The pore sizes of these MOFs were examined by fitting nonlocal density functional theory models to the N_2 adsorption isotherms (Supporting Information, section S4, Figure S19). The estimated values are in line with the pore aperture metrics derived from the crystal structures (Supporting Information, section S4, Table S5).

After establishing the permanent porosity, the CO_2 sorption properties were evaluated. Accordingly, CO_2 isotherms were

then measured at 273, 283, and 298 K (Supporting Information, section S4, Figures S20−S22). All members of the series displayed moderate CO_2 uptake at 800 Torr with MOF-892 and MOF-893, exhibiting capacities similar to one another (~23 cm^3 g^{-1}, 298 K). As expected, MOF-894 showed a lower total CO_2 uptake (19 cm^3 g^{-1}, 298 K) (Supporting Information, Figure S22). The coverage-dependent isosteric heat of adsorption (Q_{st}) of CO_2 was calculated by fitting the corresponding isotherms at 273, 283, and 298 K using a virial-type expansion equation (Supporting Information, section S5, Figure S23).[57] The CO_2 adsorption enthalpies at zero coverage for MOF-892, MOF-893, and MOF-894 were found to be 24, 31, and 32 kJ mol^{-1}, respectively.

3.3. Catalytic Cycloaddition of CO_2 to Epoxides. When carefully evaluating the structures of these MOFs, we noted four attractive features: (i) the presence of Lewis acid sites derived from accessible metal sites (Zr and In); (ii) Brønsted acid sites originating from protonated carboxylic acid moieties within the frameworks[58−60] of MOF-892 and MOF-893; (iii) the permanent porosities with large, open, and available channels, which can enable, and even enhance, substrate diffusion; and (iv) the ability to adsorb considerable amounts of CO_2 at ambient temperature. To gain insight about the nature of the pore channels for substrate diffusion purposes, the size of styrene oxide, the largest substrate, was optimized using Gaussian 09 at the B3LYP/6-311G(d,p)[61] level. Accordingly, the pore aperture metrics of MOF-892 (24 × 27 $Å^2$) and MOF-893 (8.6 × 9.9 $Å^2$) are larger than that of styrene oxide (4.3 × 7.3 $Å^2$). This supports the possibility for substrate diffusion within the MOF pore channels. The pore aperture of MOF-894 is filled with counterions, which, consequentially, restrict diffusion of the substrate. This means that catalysis for MOF-894 will only take place on the surface. With these features in hand, we decided to evaluate the new materials as heterogeneous catalysts in the cycloaddition of CO_2 to epoxides to yield cyclic organic carbonates.

To optimize the reaction conditions, we first used MOF-892, MOF-893, and MOF-894 as catalysts in a model reaction: the formation of styrene carbonate from styrene oxide and CO_2 (Table 1). Accordingly, MOF-892 demonstrates highly efficient catalytic activity (a conversion of 96%, a selectivity of 86%, and a yield of 82%) in forming styrene carbonate under a CO_2 pressure of 1 atm after 16 h at 80 °C (Table 1, entry 1). MOF-893 and MOF-894 exhibit higher selectivity toward styrene carbonate (96 and 99%, respectively), but they display lower conversions of styrene oxide (66−67%). We speculate that the higher surface area and larger pore size of MOF-892 have a positive effect in the conversion of styrene oxide, whereas the larger Q_{st} values of MOF-893 and MOF-894 benefit the selectivity for styrene carbonate formation. MOF-893 and MOF-894 promote the catalytic transformations with longer reaction times and afford conversions of 98 and 86%, respectively. When the same reaction conditions were employed in the absence of catalyst, a low yield of styrene carbonate of 19% was found. It is noted that to ensure reproducibility, all catalytic experiments were performed at least three times and the results obtained carry standard deviations of ±1, ±3, and ±2% for the conversion, selectivity, and yield of the carbonate synthesis, respectively.

The activity of the most efficient catalyst in the series, MOF-892, was then evaluated in more depth. As such, high catalytic activity was also observed for the cycloaddition of CO_2 with various epoxide substrates to produce corresponding cyclic

Table 1. Optimization of Reaction Conditions for Cycloaddition of CO_2 with Styrene Oxide Catalyzed by MOF-892, MOF-893, and MOF-894[a]

#	catalyst	t/h	con./%[b]	sel./%[b]	yield/%[b]
1	MOF-892	16	96	86	82
2	MOF-893	16	66	96	63
3	MOF-893	23	98	90	88
4	MOF-894	16	67	99	66
5	MOF-894	20	86	91	78
6	H_6CPB	16	79	24	19
7	H_6CPB[c]	16	23	86	20
8	none	16	55	88	48

[a]Reaction conditions: styrene oxide (6.87 mmol), MOF/catalyst (0.32 mol %), 1 atm CO_2 (balloon pressure), 80 °C, and nBu$_4$NBr (1 mol %). [b]Catalytic conversion (Con.), selectivity (Sel.), and yield were determined by GC−FID analysis using biphenyl as the internal standard. [c]0.16 mol % catalyst.

organic carbonates under mild reaction conditions (Table 2). Specifically, propylene oxide reacts at room temperature, 1 atm CO_2, and with an increase of nBu$_4$NBr from 5 to 8 mol %

Table 2. Optimization of Reaction for Cycloaddition of CO_2 with Various Epoxides and Base Cocatalysts Catalyzed by MOF-892[a]

#	Sub-strate	Co-catalyst	t / h	Con. / %[b]	Sel. / %[b]	Yield / %[b]
1[c]		nBu$_4$NBr	60	78	56	44
2[d]		nBu$_4$NBr	60	100	70	70
3		nBu$_4$NBr	42	70	58	40
4[c]		nBu$_4$NBr	42	78	78	61
5		nBu$_4$NCl	18	95	70	66
6		HTAB	20	99	88	87
7		DPIC	20	98	62	61
8		DMAP	30	83	35	29

[a]Reaction conditions: epoxide (6.87 mmol), MOF-892 (0.32 mol %), 1 atm CO_2 (balloon pressure), 80 °C (25 °C for propylene oxide), and cocatalyst (1 mol %). [b]Catalytic conversion (Con.), selectivity (Sel.), and yield were determined by GC−FID analysis using biphenyl as the internal standard. [c]5 mol % cocatalyst. [d]8 mol % cocatalyst. nBu$_4$NCl: tetrabutylammonium chloride, HTAB: hexadecyltrimethylammonium bromide, DPIC: 1,3-bis(2,6-diisopropylphenyl)-imidazolium chloride, and DMAP: 4-dimethylaminopyridine.

yielding 44−79% propylene carbonate after 60 h. Furthermore, cyclohexene oxide, a relatively unreactive substrate, is transformed to cyclohexene carbonate (with cis configuration) in an exceptional 61% yield using 5 mol % nBu$_4$NBr after 42 h (Table 2). Additionally, we also evaluated the influence of the cocatalysts. Entries 5−8 in Table 2 summarize the high activity of MOF-892 along with a range of bases used as cocatalysts in the cycloaddition of CO$_2$ with styrene oxide. High conversion for styrene oxide under the optimized conditions was obtained with all basic salts used as cocatalysts in the reactions, namely, tetrabutylammonium chloride (nBu$_4$NCl), hexadecyltrimethylammonium bromide (HTAB), 1,3-bis(2,6-diisopropylphenyl)imidazolium chloride (DPIC), and 4-dimethylaminopyridine (DMAP). When comparing the selectivity and yield of styrene carbonate, HTAB produced a higher selectivity and yield after 20 h than nBu$_4$NCl and DPIC with the lowest selectivity and yield coming from the DMAP cocatalyst. In short, the MOF-892/nBu$_4$NBr combination was found to be the most effective catalytic system for chemical fixation of CO$_2$ under relatively mild conditions.

To assess the heterogeneous nature of the MOF catalysts, we again performed the model reaction using optimized reaction conditions for each MOF to ensure that the catalytic activities do not originate from leaching of any metal ions from the MOF structures. At the outset of 1 to 2 h, the MOF catalysts were removed by centrifugation and the respective reaction was allowed to continue. As expected, there was no significant increase in the formation of styrene carbonate detected after the MOF catalyst was removed (Supporting Information, section S7, Figures S36−S38). At the culmination of the reaction, inductively coupled plasma mass spectrometry analysis was performed on the reaction mixture filtrate, which revealed that the concentration of Zr^{4+} or In^{3+} was <3 ppm. Indeed, this result provides strong support for the fact that the catalytic reaction was heterogeneous in nature.

Recycling studies were then undertaken using the optimized conditions (Supporting Information, section S7). In a model reaction, an MOF-892 catalyst was reused up to five successive times with the average yield of 83% styrene carbonate (Supporting Information, Figure S39). Similarly, MOF-893 was reused up to four times with the yield of styrene carbonate decreasing from 84.9% (average) to 69.0% (after the fifth reaction) (Supporting Information, Figure S40). Finally, the activity of recycled MOF-894 was retained with an average yield of 79.5% after three consecutive reactions (Supporting Information, Figure S41). PXRD analysis was performed on all of the recycled MOF catalysts, in which structural maintenance was proven (Supporting Information, section S9, Figures S42−S44). Additionally, FT-IR analyses (Supporting Information, Figures S45−S47) and scanning electron microscopy imaging (Supporting Information, Figures S48−S50) of MOF-892, MOF-893, and MOF-894 provided further evidence that these MOFs maintained their structural integrity and well-defined morphology. To evaluate the surface acidic/basic properties of MOF-892, MOF-893, and MOF-894, FT-IR analyses were performed on both freshly prepared and recycled MOF materials using adsorbed pyridine. (Supporting Information, Figures S51−S53).[31,62] As such, the FT-IR spectra of fresh and recycled MOF-892 and MOF-893 exhibited the presence of both Brønsted (1712−1691 and 1536−1515 cm$^{−1}$) and Lewis acid sites (1586−1581 and 1402−1400 cm$^{−1}$). This indicated that the acidic properties of MOF-892 and MOF-893 remained even after they were used in consecutive reactions. It is noted

that the basic sites (1654 cm$^{−1}$) in recycled MOF-894 were observed to have vanished, which provides evidences for the decrease in the catalytic performance after the third cycle reaction.

To demonstrate the superiority of these MOF catalysts, we performed the cycloaddition of CO$_2$ with styrene oxide using other homogeneous and heterogeneous acid-based catalysts, including other Lewis acidic-MOF materials (Table 3). The

Table 3. Comparative Study of Various Catalysts for Cycloaddition of CO$_2$ with Styrene Oxide[a]
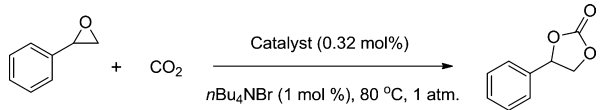
type	catalyst	S_{BET}/m^2 g$^{−1}$	con./%[b]	sel./%[b]	yield/%[b]
MOF	MOF-892	1904	96	86	82
	MOF-893	558	66	96	63
	MOF-894	5	67	99	66
	MOF-890[c]	300	59	100	59
	HKUST-1	1334	55	76	42
	ZIF-8	1500	32	81	26
	MOF-177	2344	71	87	62
	MIL-53(Al)	710	37	91	33
	UiO-67[c]	2179	63	80	50
	Mg-MOF-74[c]	1297	26	100	26
hetero.	Y-zeolite	589	55	85	46
	silica−alumina	226	80	73	58
	Al$_2$O$_3$		72	80	58
homo.	CaCl$_2$		65	78	51
	ZrCl$_4$		68	74	50
	ZrOCl$_2$·8H$_2$O		70	45	32
	In(NO$_3$)$_3$·xH$_2$O		21	94	19

[a]Reaction conditions: styrene oxide (6.87 mmol), MOF/catalyst (0.32 mol % ratio, based on molecular weight), 1 atm CO$_2$ (balloon pressure), nBu$_4$NBr (1 mol %), 80 °C, 16 h. [b]Catalytic conversion (Con.), selectivity (Sel.), and yield were determined by GC−FID analysis using biphenyl as the internal standard. [c]Molecular weight calculated from [Cu$_3$(CPB)(DMF)$_{0.5}$]·6H$_2$O, Zr$_6$O$_4$(OH)$_4$(C$_{12}$N$_2$O$_4$H$_6$)$_6$, and Mg$_2$(C$_8$O$_6$H$_2$)(H$_2$O)$_2$ for MOF-890, UiO-67-bpydc, and Mg-MOF-74, respectively. Hetero. = heterogeneous; and Homo. = homogeneous.

experiments show that MOF-892 is the best performer over other benchmark catalysts. In general, the homogeneous metal salts, CaCl$_2$, ZrCl$_4$, ZrOCl$_2$·8H$_2$O, and In(NO$_3$)$_3$·xH$_2$O, exhibited lower yields of 51, 50, 32, and 19%, respectively, than those of MOF-892. Additionally, commercial acid-based platforms functioning as comparative heterogeneous catalysts, such as silica−alumina, Y-zeolite, and aluminum oxide, were also lower performers with ca. 46−58% yields obtained. Similarly, the MOF-based catalysts, ZIF-8,[63] Mg-MOF-74,[64] HKUST-1,[65] and Al-MIL-53,[66] exhibited lower yields of 26, 26, 33, and 42%, respectively, under identical conditions. In addition, MOF-177[57] and UiO-67-bpydc[67] promoted the cycloaddition reaction with moderate yields of 62 and 50%, respectively. Finally, MOF-890,[37] a layered copper-based MOF constructed from H$_6$CPB linker, and MOF-894 proceed with exceptional selectivity for styrene carbonate formation (>99%). This selectivity result is attributed to these materials' highly selective CO$_2$ adsorption at low-coverage pressure. Their moderate conversions and corresponding yields (59−66%) for

Scheme 2. Proposed Mechanism for the Synthesis of Styrene Carbonate Catalyzed by MOF-892
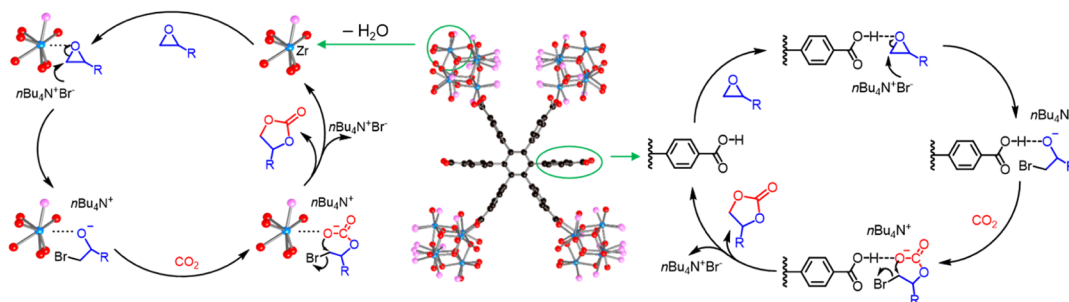
the styrene carbonate synthesis of these layer-based MOFs are due to the lower surface areas or limited porosities repelling the diffusion of reactants.

Several factors may influence the activity of heterogeneous catalysts for the chemical fixation of CO_2 under mild conditions (80 °C and 1 atm of CO_2). These include surface area, affinity toward CO_2, and accessibility of multiple active sites. In light of the comparative studies, it can be seen that high surface area and high CO_2 total uptake at room temperature are not determining factors in improving the activity of catalysts. This is evidenced by higher yields achieved by MOF-892 (BET = 1904 m^2 g^{-1}/total CO_2 uptake at 298 K = 23 cm^3 g^{-1}) compared to other representative porous MOFs, such as MOF-177 (2300 m^2 g^{-1}/12 cm^3 g^{-1}, respectively), UiO-67-bpydc (2180 m^2 g^{-1}/33 cm^3 g^{-1}, respectively), ZIF-8 (1500 m^2 g^{-1}/16 cm^3 g^{-1}, respectively), HKUST-1 (1330 m^2 g^{-1}/107 cm^3 g^{-1}, respectively), and Mg-MOF-74 (1300 m^2 g^{-1}/130 cm^3 g^{-1}, respectively) (Supporting Information, Figures S27 and S28, Table S6). On the other hand, MOF-892 is one of the few examples of MOFs combining Lewis and Brønsted active acid sites, which are accessible through their large hexagonal channels. The activity of the Brønsted acid sites was proven by performing a model reaction using H_6CPB as a homogeneous catalyst, in a concentration equivalent to that provided by MOF-892, considering that each linker in the MOF provides two free carboxylic acid groups. As such, a yield of 49% was obtained, proving that the cycloaddition of CO_2 can also be catalyzed by Brønsted acids.

The epoxide substrates were effectively activated due to the coexistence of two types of active sites in MOF-892 (Lewis acid sites from accessible Zr units and Brønsted acid sites from protonated carboxylic acid moieties). On this basis, a plausible mechanism for the cycloaddition of CO_2 to epoxides, as catalyzed by MOF-892, can be proposed (Scheme 2). Accordingly, the Zr centers and protonated carboxylic acid moieties of activated MOF-892 are first involved in the coordination of the epoxide substrate. Thereafter, the Br^- ion of the cocatalyst nBu$_4$NBr engages in a nucleophilic attack on the epoxide, leading to ring opening. The O atom of the ring-opened epoxide then reacts with CO_2, thus resulting in the generation of a metal-carbonate intermediate. Finally, an intramolecular ring closure occurs, in which a cyclic carbonate is formed and the catalyst is regenerated. This plausible mechanism for MOF-892 reveals a synergistic effect because of the presence of both active Lewis and Brønsted acid sites, in promoting the reaction.

3.4. Postsynthetic Methylation of MOF-892. To gain insight into the role of the free carboxylic acid group, we methylated the free carboxylic acids in MOF-892 to remove the effect of Brønsted acidity resulting from the carboxylic

groups. The introduction of methyl esters within the framework of MOF-892 is rationally expected to prevent the contribution of these Brønsted acid sites in the catalysis. After the reaction of the activated MOF-892 with a solution of TMS-CHN$_2$ at 273 K, the methylated MOF-892 (denoted Me-MOF-892) was activated by following the same activation procedures as that of the parent MOF-892. The resulting crystals of Me-MOF-892 (Supporting Information, Figure S54) were characterized by PXRD, ^{1}H NMR, EA, FT-IR, and TGA analyses (Supporting Information, section S10).

The PXRD pattern of Me-MOF-892 samples reveals that the as-synthesized and activated frameworks retain their crystallinity and hexagonal lattice system (Supporting Information, Figure S55). ^{1}H NMR analysis of digested Me-MOF-892 in a 20% DCl/DMSO-d_6 solution indicated the presence of methyl ester group with a new peak at 3.67 ppm. The relative integration of the peaks reveals a quantitative methylation of the two free carboxylic groups (Supporting Information, Figure S56). Furthermore, EA confirmed these results obtained from ^{1}H digestion NMR (calcd for $Zr_6O_4(OH)_4(CPB-(CH_3)_2)_{1.5}(CH_3CO_2)_2(DMF)_{0.2}(H_2O)_{15}$: C, 41.27; H, 3.74; N, 0.12%. Found: C, 41.27; H, 3.47; N, 0.57%). FT-IR spectra of Me-MOF-892 were obtained to compare the coordinated vibration frequencies to that of MOF-892 (Supporting Information, Figure S57). Accordingly, the O−H stretching frequencies (3411 cm^{-1} for MOF-892) shifted to lower wavenumbers (3356 cm^{-1} for Me-MOF-892), and the O−H absorption region of Me-MOF was found to be less broad than what was observed in the corresponding acids. Indeed, this is expected due to the incorporation of the methyl group in the carboxylate moiety. The C−OH bending vibrations of the carboxyl group shifted from 1258 cm^{-1} for MOF-892 to the higher wavenumber of 1276 cm^{-1} for Me-MOF-892 in accordance with the formation of esters. Analysis of the weight percent of residual metal oxide for Me-MOF-892 (35.9%) following TGA analysis (Supporting Information, Figure S58) was also found to be consistent with the calculated value derived from the EA (35.2%).

To assess the solvent-free material, crystals of Me-MOF-892 were washed with MeOH (3 × 5 mL) before drying under the same conditions as the parent MOF-892 via supercritical CO_2 activation. Subsequently, a N$_2$ adsorption isotherm at 77 K and CO_2 adsorption isotherm at 273 K were measured for Me-MOF-892 to verify its permanent porosity and CO_2 adsorption properties. Me-MOF-892 exhibited a lower BET surface area (1300 m^2 g^{-1}) and a lower total CO_2 uptake (34 cm^3 g^{-1}) than those found for the parent MOF-892 (Supporting Information, Figures S59 and S60). Finally, the catalytic activity of Me-MOF-892 was illustrated using the model reaction. As expected, Me-MOF-892 has a lower catalytic performance in

Table 4. One-Pot Synthesis of Styrene Carbonate from Styrene and CO_2 Catalyzed by MOF-892 with the Oxidant *tert*-Butyl Hydroperoxide (TBHP)[a] and Comparative Studies
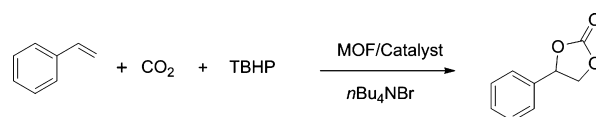
#	catalyst	TBHP/equiv[b]	nBu$_4$NBr/equiv[b]	CO_2/atm	t/h	temp/°C	con./%[c]	sel./%[c]	yield/%[c]
1	MOF-892	1.89	0.96	1	9	80	100	51	51
2	MOF-892	1.89	1.53	1	9	80	100	80	80
3[d]	ZnW-PYI1	2.0	0.01	4.9	96	50			92
4[d]	ZnW-PYI2	2.0	0.01	4.9	96	50			90
5[e]	Cr-MIL-101	1.5	0.1	7.9	24	25	39	19	
6	none	1.89	1.53	1	9	80	72	57	41

[a]Reaction conditions: styrene (1.31 mmol), MOF-892 (6 mol %), TBHP (3.92 mmol), nBu$_4$NBr, CO_2 (balloon pressure), 80 °C, 9 h. [b]Equivalent to mole of styrene. [c]The catalytic conversion (Con.), selectivity (Sel.), and yield were determined by GC–FID analysis using biphenyl as the internal standard. [d]Reference 41. [e]Reference 42.

the synthesis of styrene carbonate with a yield reaching 69% (Supporting Information, section S10, Table S7), in accordance with the absence of free carboxylic acid groups.

3.5. One-Pot Oxidative Carboxylation of Styrene and CO_2. In light of MOF-892's exceptional performance, we turned our attention to carrying out preliminary experiments for the one-pot synthesis of styrene carbonate from styrene and CO_2 in the presence of an oxidant, TBHP (Table 4). Remarkably, MOF-892 was shown again to be an efficient catalyst for this one-pot reaction at 80 °C and 1 atm CO_2 pressure, as compared to the previously reported MOF catalysts, ZnW-PYI1[41] and Cr-MIL-101.[42] Indeed, MOF-892 was able to reach 100% conversion of styrene only after 9 h. Furthermore, high selectivity (80%) and yield (80%) were also obtained when the amount of nBu$_4$NBr was increased from 0.96 to 1.53 equiv. It is noted that t-butanol and benzaldehyde were observed as by-products of the reactions.

4. SUMMARY

In summary, a new series of hexatopic linker-based MOFs, two of which are zirconium-based (MOF-892 and MOF-893) with the remaining one being indium-based (MOF-894), were prepared and fully characterized. The structures of MOF-892, MOF-893, and MOF-894 were determined to adopt **stp**, **hfp**, and **kgd** topologies, respectively. Interestingly, **hfp** is a previously unobserved topology, whereas **stp** was observed for the first time for any zirconium-based MOF. All of these new materials exhibit potential as recyclable catalysts for the heterogeneous cycloaddition of CO_2 to styrene oxide to form styrene carbonate. Each MOF demonstrates high conversion, selectivity, and yield under mild conditions (solvent-free, ambient pressure of CO_2, 80 °C for 16 h). Among them, MOF-892 was proven to be the highest performer and was also applied to the transformation of propylene oxide and cyclohexene oxide as well as in the one-pot synthesis of styrene carbonate from styrene using TBHP as the oxidant reagent in 9 h. The role of the active COOH group integrated within MOF-892 was proposed and demonstrated. The results reported herein present exciting new avenues to explore in the design and selection of MOFs for the chemical fixation of CO_2 to epoxides and olefins under mild conditions.

■ ASSOCIATED CONTENT

ⓢ Supporting Information

The Supporting Information is available free of charge on the ACS Publications website at DOI: 10.1021/acsami.7b16163.

> Crystallographic data of MOF-892 (CIF)
> Crystallographic data of MOF-893 (CIF)
> Crystallographic data of MOF-894 (CIF)
> Full MOF synthetic details and characterization (including PXRD, TGA curves, FT-IR, and adsorption isotherms) and catalytic reaction details (PDF)

■ AUTHOR INFORMATION

Corresponding Author
*E-mail: gandara@icmm.csic.es.

ORCID ⓘ
Huong T. D. Nguyen: 0000-0002-7965-9742
Kyle E. Cordova: 0000-0002-4988-0497
Felipe Gándara: 0000-0002-1671-6260

Author Contributions
#P.T.K.N. and H.T.D.N. contributed equally.

■ REFERENCES

(1) Furukawa, H.; Cordova, K. E.; O'Keeffe, M.; Yaghi, O. M. The Chemistry and Applications of Metal-Organic Frameworks. *Science* **2013**, *341*, 1230444.

(2) Li, M.; Li, D.; O'Keeffe, M.; Yaghi, O. M. Topological Analysis of Metal−Organic Frameworks with Polytopic Linkers and/or Multiple Building Units and the Minimal Transitivity Principle. *Chem. Rev.* **2014**, *114*, 1343−1370.

(3) Reinares-Fisac, D.; Aguirre-Díaz, L. M.; Iglesias, M.; Snejko, N.; Gutiérrez-Puebla, E.; Monge, M. Á.; Gándara, F. A Mesoporous Indium Metal−Organic Framework: Remarkable Advances in Catalytic Activity for Strecker Reaction of Ketones. *J. Am. Chem. Soc.* **2016**, *138*, 9089−9092.

(4) Aguirre-Díaz, L. M.; Gándara, F.; Iglesias, M.; Snejko, N.; Gutiérrez-Puebla, E.; Monge, M. Á. Tunable Catalytic Activity of Solid Solution Metal−Organic Frameworks in One-Pot Multi-component Reactions. *J. Am. Chem. Soc.* **2015**, *137*, 6132−6135.

(5) Feng, D.; Gu, Z.-Y.; Chen, Y.-P.; Park, J.; Wei, Z.; Sun, Y.; Bosch, M.; Yuan, S.; Zhou, H.-C. A Highly Stable Porphyrinic Zirconium Metal−Organic Framework with shp-a Topology. *J. Am. Chem. Soc.* **2014**, *136*, 17714−17717.

(6) Li, P.; Modica, J. A.; Howarth, A. J.; Vargas, L. E.; Moghadam, P. Z.; Snurr, R. Q.; Mrksich, M.; Hupp, J. T.; Farha, O. K. Toward Design Rules for Enzyme Immobilization in Hierarchical Mesoporous Metal-Organic Frameworks. *Chem* **2016**, *1*, 154−169.

(7) Bai, Y.; Dou, Y.; Xie, L.-H.; Rutledge, W.; Li, J.-R.; Zhou, H.-C. Zr-Based Metal−Organic Frameworks: Design, Synthesis, Structure, and Applications. *Chem. Soc. Rev.* **2016**, *45*, 2327−2367.

(8) Cavka, J. H.; Jakobsen, S.; Olsbye, U.; Guillou, N.; Lamberti, C.; Bordiga, S.; Lillerud, K. P. A New Zirconium Inorganic Building Brick Forming Metal Organic Frameworks with Exceptional Stability. *J. Am. Chem. Soc.* **2008**, *130*, 13850−13851.

(9) Wang, T. C.; Bury, W.; Gómez-Gualdrón, D. A.; Vermeulen, N. A.; Mondloch, J. E.; Deria, P.; Zhang, K.; Moghadam, P. Z.; Sarjeant, A. A.; Snurr, R. Q.; Stoddart, J. F.; Hupp, J. T.; Farha, O. K. Ultrahigh Surface Area Zirconium MOFs and Insights into the Applicability of the BET Theory. *J. Am. Chem. Soc.* **2015**, *137*, 3585−3591.

(10) Trickett, C. A.; Gagnon, K. J.; Lee, S.; Gándara, F.; Bürgi, H.-B.; Yaghi, O. M. Definitive Molecular Level Characterization of Defects in UiO-66 Crystals. *Angew. Chem., Int. Ed.* **2015**, *54*, 11162−11167.

(11) Furukawa, H.; Gándara, F.; Zhang, Y.-B.; Jiang, J.; Queen, W. L.; Hudson, M. R.; Yaghi, O. M. Water Adsorption in Porous Metal−Organic Frameworks and Related Materials. *J. Am. Chem. Soc.* **2014**, *136*, 4369−4381.

(12) Morris, W.; Volosskiy, B.; Demir, S.; Gándara, F.; McGrier, P. L.; Furukawa, H.; Cascio, D.; Stoddart, J. F.; Yaghi, O. M. Synthesis, Structure, and Metalation of Two New Highly Porous Zirconium Metal−Organic Frameworks. *Inorg. Chem.* **2012**, *51*, 6443−6445.

(13) Jiang, H.-L.; Feng, D.; Wang, K.; Gu, Z.-Y.; Wei, Z.; Chen, Y.-P.; Zhou, H.-C. An Exceptionally Stable, Porphyrinic Zr Metal−Organic Framework Exhibiting pH-Dependent Fluorescence. *J. Am. Chem. Soc.* **2013**, *135*, 13934−13938.

(14) Feng, D.; Chung, W.-C.; Wei, Z.; Gu, Z.-Y.; Jiang, H.-L.; Chen, Y.-P.; Darensbourg, D. J.; Zhou, H.-C. Construction of Ultrastable Porphyrin Zr Metal−Organic Frameworks through Linker Elimi-nation. *J. Am. Chem. Soc.* **2013**, *135*, 17105−17110.

(15) Jiang, J.; Gándara, F.; Zhang, Y.-B.; Na, K.; Yaghi, O. M.; Klemperer, W. G. Superacidity in Sulfated Metal−Organic Frame-work-808. *J. Am. Chem. Soc.* **2014**, *136*, 12844−12847.

(16) Liu, Q.; Wu, L.; Jackstell, R.; Beller, M. Using Carbon Dioxide as a Building Block in Organic Synthesis. *Nat. Commun.* **2015**, *6*, 5933.

(17) Trickett, C. A.; Helal, A.; Al-Maythalony, B. A.; Yamani, Z. H.; Cordova, K. E.; Yaghi, O. M. The Chemistry of Metal−Organic Frameworks for CO₂ Capture, Regeneration and Conversion. *Nat. Rev. Mater.* **2017**, *2*, 17045.

(18) Martín, C.; Fiorani, G.; Kleij, A. W. Recent Advances in the Catalytic Preparation of Cyclic Organic Carbonates. *ACS Catal.* **2015**, *5*, 1353−1370.

(19) Calabrese, C.; Liotta, L. F.; Carbonell, E.; Giacalone, F.; Gruttadauria, M.; Aprile, C. Imidazolium-Functionalized Carbon Nanohorns for the Conversion of Carbon Dioxide: Unprecedented Increase of Catalytic Activity after Recycling. *ChemSusChem* **2017**, *10*, 1202−1209.

(20) Li, C.-G.; Xu, L.; Wu, P.; Wu, H.; He, M. Efficient Cycloaddition of Epoxides and Carbon Dioxide over Novel Organic-Inorganic Hybrid Zeolite Catalysts. *Chem. Commun.* **2014**, *50*, 15764−15767.

(21) Meng, X.; He, H.; Nie, Y.; Zhang, X.; Zhang, S.; Wang, J. Temperature-Controlled Reaction−Separation for Conversion of CO₂ to Carbonates with Functional Ionic Liquids Catalyst. *ACS Sustainable Chem. Eng.* **2017**, *5*, 3081−3086.

(22) D'Elia, V.; Dong, H.; Rossini, A. J.; Widdifield, C. M.; Vummaleti, S. V. C.; Minenkov, Y.; Poater, A.; Abou-Hamad, E.; Pelletier, J. D. A.; Cavallo, L.; Emsley, L.; Basset, J.-M. Cooperative Effect of Monopodal Silica-Supported Niobium Complex Pairs Enhancing Catalytic Cyclic Carbonate Production. *J. Am. Chem. Soc.* **2015**, *137*, 7728−7739.

(23) Yang, Z.; Yu, B.; Zhang, H.; Zhao, Y.; Chen, Y.; Ma, Z.; Ji, G.; Gao, X.; Han, B.; Liu, Z. Metalated Mesoporous Poly-(Triphenylphosphine) with Azo Functionality: Efficient Catalysts for CO₂ Conversion. *ACS Catal.* **2016**, *6*, 1268−1273.

(24) Li, P.-Z.; Wang, X.-J.; Liu, J.; Lim, J. S.; Zou, R.; Zhao, Y. A Triazole-Containing Metal−Organic Framework as a Highly Effective and Substrate Size-Dependent Catalyst for CO₂ Conversion. *J. Am. Chem. Soc.* **2016**, *138*, 2142−2145.

(25) Guo, X.; Zhou, Z.; Chen, C.; Bai, J.; He, C.; Duan, C. New Rht-Type Metal−Organic Frameworks Decorated with Acylamide Groups for Efficient Carbon Dioxide Capture and Chemical Fixation from Raw Power Plant Flue Gas. *ACS Appl. Mater. Interfaces* **2016**, *8*, 31746−31756.

(26) Beyzavi, M. H.; Klet, R. C.; Tussupbayev, S.; Borycz, J.; Vermeulen, N. A.; Cramer, C. J.; Stoddart, J. F.; Hupp, J. T.; Farha, O. K. A Hafnium-Based Metal−Organic Framework as an Efficient and Multifunctional Catalyst for Facile CO₂ Fixation and Regioselective and Enantioretentive Epoxide Activation. *J. Am. Chem. Soc.* **2014**, *136*, 15861−15864.

(27) Beyzavi, M. H.; Stephenson, C. J.; Liu, Y.; Karagiaridi, O.; Hupp, J. T.; Farha, O. K. Metal-Organic Framework-Based Catalysts: Chemical Fixation of CO₂ with Epoxides Leading to Cyclic Organic Carbonates. *Front. Energy Res.* **2015**, *2*, 63.

(28) Miralda, C. M.; Macias, E. E.; Zhu, M.; Ratnasamy, P.; Carreon, M. A. Zeolitic Imidazole Framework-8 Catalysts in the Conversion of CO₂ to Chloropropene Carbonate. *ACS Catal.* **2012**, *2*, 180−183.

(29) Macias, E. E.; Ratnasamy, P.; Carreon, M. A. Catalytic Activity of Metal Organic Framework Cu₃(BTC)₂ in the Cycloaddition of CO₂ to Epichlorohydrin Reaction. *Catal. Today* **2012**, *198*, 215−218.

(30) Zhu, M.; Carreon, M. A. Porous Crystals as Active Catalysts for the Synthesis of Cyclic Carbonates. *J. Appl. Polym. Sci.* **2014**, *131*, 39738.

(31) Zhu, M.; Srinivas, D.; Bhogeswararao, S.; Ratnasamy, P.; Carreon, M. A. Catalytic Activity of ZIF-8 in the Synthesis of Styrene Carbonate from CO₂ and Styrene Oxide. *Catal. Commun.* **2013**, *32*, 36−40.

(32) Liu, L.; Wang, S.-M.; Han, Z.-B.; Ding, M.; Yuan, D.-Q.; Jiang, H.-L. Exceptionally Robust In-Based Metal-Organic Framework for Highly Efficient Carbon Dioxide Capture and Conversion. *Inorg. Chem.* **2016**, *55*, 3558−3565.

(33) Li, P.-Z.; Wang, X.-J.; Liu, J.; Phang, H. S.; Li, Y.; Zhao, Y. Highly Effective Carbon Fixation via Catalytic Conversion of CO₂ by an Acylamide-Containing Metal−Organic Framework. *Chem. Mater.* **2017**, *29*, 9256−9261.

(34) Maina, J. W.; Pozo-Gonzalo, C.; Kong, L.; Schütz, J.; Hill, M.; Dumée, L. F. Metal organic framework based catalysts for CO₂ conversion. *Mater. Horiz.* **2017**, *4*, 345−361.

743

(35) Yao, B.-J.; Ding, L.-G.; Li, F.; Li, J.-T.; Fu, Q.-J.; Ban, Y.; Guo, A.; Dong, Y.-B. Chemically Cross-Linked MOF Membrane Generated from Imidazolium-Based Ionic Liquid-Decorated UiO-66 Type NMOF and Its Application toward CO_2 Separation and Conversion. *ACS Appl. Mater. Interfaces* 2017, 9, 38919−38930.

(36) North, M.; Pasquale, R.; Young, C. Synthesis of Cyclic Carbonates from Epoxides and CO_2. *Green Chem.* 2010, 12, 1514−1539.

(37) Wang, J.-L.; Wang, J.-Q.; He, L.-N.; Dou, X.-Y.; Wu, F. A CO_2/H_2O_2-Tunable Reaction: Direct Conversion of Styrene into Styrene Carbonate Catalyzed by Sodium Phosphotungstate/N-Bu₄NBr. *Green Chem.* 2008, 10, 1218−1223.

(38) Wu, J.; Kozak, J. A.; Simeon, F.; Hatton, T. A.; Jamison, T. F. Mechanism-Guided Design of Flow Systems for Multicomponent Reactions: Conversion of CO_2 and Olefins to Cyclic Carbonates. *Chem. Sci.* 2014, 5, 1227−1231.

(39) Vara, B. A.; Struble, T. J.; Wang, W.; Dobish, M. C.; Johnston, J. N. Enantioselective Small Molecule Synthesis by Carbon Dioxide Fixation Using a Dual Brønsted Acid/Base Organocatalyst. *J. Am. Chem. Soc.* 2015, 137, 7302−7305.

(40) Nguyen, P. T. K.; Nguyen, H. T. D.; Pham, H. Q.; Kim, J.; Cordova, K. E.; Furukawa, H. Synthesis and Selective CO_2 Capture Properties of a Series of Hexatopic Linker-Based Metal−Organic Frameworks. *Inorg. Chem.* 2015, 54, 10065−10072.

(41) Han, Q.; Qi, B.; Ren, W.; He, C.; Niu, J.; Duan, C. Polyoxometalate-Based Homochiral Metal-Organic Frameworks for Tandem Asymmetric Transformation of Cyclic Carbonates from Olefins. *Nat. Commun.* 2015, 6, 10007.

(42) Zalomaeva, O. V.; Maksimchuk, N. V.; Chibiryaev, A. M.; Kovalenko, K. A.; Fedin, V. P.; Balzhinimaev, B. S. Synthesis of Cyclic Carbonates from Epoxides or Olefins and CO_2 Catalyzed by Metal-Organic Frameworks and Quaternary Ammonium Salts. *J. Energy Chem.* 2013, 22, 130−135.

(43) Bruker APEX3, v2015.5-2; Bruker AXS Inc.: Madison, WI, U.S.A., 2015.

(44) Bruker. SAINT, v8.37A; Bruker AXS Inc.: Madison, WI, USA, 2015.

(45) Bruker. SADABS, 2016/2; Bruker AXS Inc.: Madison, WI, USA, 2016.

(46) Sheldrick, G. M. A Short History of Shelx. *Acta Crystallogr., Sect. A: Found. Crystallogr.* 2008, 64, 112−122.

(47) Dolomanov, O. V.; Bourhis, L. J.; Gildea, R. J.; Howard, J. A. K.; Puschmann, H. Olex2: A Complete Structure Solution, Refinement and Analysis Program. *J. Appl. Crystallogr.* 2009, 42, 339−341.

(48) Blatov, V. A.; Shevchenko, A. P.; Proserpio, D. M. Applied Topological Analysis of Crystal Structures with the Program Package Topospro. *Cryst. Growth Des.* 2014, 14, 3576−3586.

(49) Wang, R.; Wang, Z.; Xu, Y.; Dai, F.; Zhang, L.; Sun, D. Porous Zirconium Metal−Organic Framework Constructed from 2D → 3D Interpenetration Based on a 3,6-Connected Kgd Net. *Inorg. Chem.* 2014, 53, 7086−7088.

(50) Ma, J.; Wong-Foy, A. G.; Matzger, A. J. The Role of Modulators in Controlling Layer Spacings in a Tritopic Linker Based Zirconium 2D Microporous Coordination Polymer. *Inorg. Chem.* 2015, 54, 4591−4593.

(51) Alezi, D.; Spanopoulos, I.; Tsangarakis, C.; Shkurenko, A.; Adil, K.; Belmabkhout, Y.; O'Keeffe, M.; Eddaoudi, M.; Trikalitis, P. N. Reticular Chemistry at Its Best: Directed Assembly of Hexagonal Building Units into the Awaited Metal-Organic Framework with the Intricate Polybenzene Topology, pbz-MOF. *J. Am. Chem. Soc.* 2016, 138, 12767−12770.

(52) Feng, D.; Wang, K.; Su, J.; Liu, T.-F.; Park, J.; Wei, Z.; Bosch, M.; Yakovenko, A.; Zou, X.; Zhou, H.-C. A Highly Stable Zeotype Mesoporous Zirconium Metal-Organic Framework with Ultralarge Pores. *Angew. Chem., Int. Ed.* 2015, 54, 149−154.

(53) O'Keeffe, M.; Peskov, M. A.; Ramsden, S. J.; Yaghi, O. M. The Reticular Chemistry Structure Resource (RCSR) Database of, and Symbols for, Crystal Nets. *Acc. Chem. Res.* 2008, 41, 1782−1789.

(54) Spek, A. L. Structure Validation in Chemical Crystallography. *Acta Crystallogr., Sect. D: Biol. Crystallogr.* 2009, 65, 148−155.

(55) Delgado-Friedrichs, O.; O'Keeffe, M. Identification of and Symmetry Computation for Crystal Nets. *Acta Crystallogr., Sect. A: Found. Crystallogr.* 2003, 59, 351−360.

(56) Aguirre-Díaz, L. M.; Reinares-Fisac, D.; Iglesias, M.; Gutiérrez-Puebla, E.; Gándara, F.; Snejko, N.; Monge, M. A. Group 13th Metal-Organic Frameworks and Their Role in Heterogeneous Catalysis. *Coord. Chem. Rev.* 2017, 335, 1−27.

(57) Furukawa, H.; Miller, M. A.; Yaghi, O. M. Independent Verification of the Saturation Hydrogen Uptake in MOF-177 and Establishment of a Benchmark for Hydrogen Adsorption in Metal-Organic Frameworks. *J. Mater. Chem.* 2007, 17, 3197−3204.

(58) Zhang, G.; Wei, G.; Liu, Z.; Oliver, S. R. J.; Fei, H. A Robust Sulfonate-Based Metal−Organic Framework with Permanent Porosity for Efficient CO_2 Capture and Conversion. *Chem. Mater.* 2016, 28, 6276−6281.

(59) Liu, L.; Wang, S.-M.; Han, Z.-B.; Ding, M.; Yuan, D.-Q.; Jiang, H.-L. Exceptionally Robust In-Based Metal-Organic Framework for Highly Efficient Carbon Dioxide Capture and Conversion. *Inorg. Chem.* 2016, 55, 3558−3565.

(60) Song, J. Y.; Ahmed, I.; Seo, P. W.; Jhung, S. H. UiO-66-Type Metal−Organic Framework with Free Carboxylic Acid: Versatile Adsorbents Via H-Bond for Both Aqueous and Nonaqueous Phases. *ACS Appl. Mater. Interfaces* 2016, 8, 27394−27402.

(61) Frisch, M. J.; Trucks, G. W.; Schlegel, H. B.; Scuseria, G. E.; Robb, M. A.; Cheeseman, J. R.; Scalmani, G.; Barone, V.; Mennucci, B.; Petersson, G. A. *Gaussian 09*, Revisions D.01 and B.01; Gaussian, Inc.: Wallingford, CT, 2010.

(62) Barzetti, T.; Selli, E.; Moscotti, D.; Forni, L. Pyridine and Ammonia as Probes for Ftir Analysis of Solid Acid Catalysts. *J. Chem. Soc., Faraday Trans.* 1996, 92, 1401−1407.

(63) Wang, B.; Côté, A. P.; Furukawa, H.; O'Keeffe, M.; Yaghi, O. M. Colossal Cages in Zeolitic Imidazolate Frameworks as Selective Carbon Dioxide Reservoirs. *Nature* 2008, 453, 207−211.

(64) Britt, D.; Furukawa, H.; Wang, B.; Glover, T. G.; Yaghi, O. M. Highly Efficient Separation of Carbon Dioxide by a Metal-Organic Framework Replete with Open Metal Sites. *Proc. Natl. Acad. Sci. U.S.A.* 2009, 106, 20637−20640.

(65) Furukawa, H.; Go, Y. B.; Ko, N.; Park, Y. K.; Uribe-Romo, F. J.; Kim, J.; O'Keeffe, M.; Yaghi, O. M. Isoreticular Expansion of Metal−Organic Frameworks with Triangular and Square Building Units and the Lowest Calculated Density for Porous Crystals. *Inorg. Chem.* 2011, 50, 9147−9152.

(66) Férey, G.; Latroche, M.; Serre, C.; Millange, F.; Loiseau, T.; Percheron-Guégan, A. Hydrogen Adsorption in the Nanoporous Metal-Benzenedicarboxylate $M(OH)(O_2C-C_6H_4-CO_2)$ (M = Al^{3+}, Cr^{3+}), MIL-53. *Chem. Commun.* 2003, 2976−2977.

(67) Gonzalez, M. I.; Bloch, E. D.; Mason, J. A.; Teat, S. J.; Long, J. R. Single-Crystal-to-Single-Crystal Metalation of a Metal−Organic Framework: A Route toward Structurally Well-Defined Catalysts. *Inorg. Chem.* 2015, 54, 2995−3005.